The Energetics of Surfactant-Templating of Zeolites

Noemi Linares, Erika O Jardim, Alexander Sachse, Elena Serrano, Javier García-Martínez

The Energetics of Surfactant‐Templating of Zeolites

N. Linares, E. O. Jardim, A. Sachse, E. Serrano, and J. García-Martínez*

Abstract: Mesoporosity can be conveniently introduced in zeolites by treating them in basic surfactant solutions. The apparent activation energy involved in the formation of mesopores in USY via surfactant-templating was obtained through the combination of *in situ* synchrotron XRD and *ex situ* gas adsorption. Additionally, techniques such as pH measurements and TG/DTA were employed to determine the OH^- evolution and the CTA^+ uptake during the development of mesoporosity, providing information about the different steps included in this method. By combining these *in situ* and *ex situ* techniques, we have been able, for the first time, to determine the apparent activation energies of the different processes involved in the mesostructuring of USY zeolites, which are in the same order of magnitude (30 – 65 kJ mol^{-1}) to those involved in the crystallization of zeolites. Hence, important mechanistic insights on the surfactant-templating method where obtained. 1012 Abstract Text, 800-1000 characters.

For more than 25 years now, cationic surfactants have been widely applied to prepare mesoporous amorphous materials.[1,2] Since then, researchers have made great efforts to extend the use of these surfactant-templating techniques for the preparation of mesoporous zeolites. Among the different methods used to impart secondary porosity within zeolites,[3,4] the post-synthetic treatment with cationic surfactants has proved to be an effective tool to introduce intracrystalline mesoporosity, allowing to tailor pore dimensions, while maintaining the key features of the zeolite including strong acidity and excellent hydrothermal stability.[5,6]

Recently, we reported the first time-resolved observation of the development of mesoporosity in zeolites through surfactant-templating by *in situ* XRD. [7] Indeed, the combination of the experimental data with theoretical calculations provided new insights on the formation of intracrystalline mesoporosity featuring short-range order in zeolites. Moreover, the use of Liq-TEM rendered the first *in situ* real time visualization of this process.[7]

In spite of the numerous reports dealing with surfactant-templating of zeolites [5-7] and the fact that these materials are already a commercial reality,[8] the driving forces involved in this process are still unknown, their investigation is one of the objectives of this paper A systematic study of the apparent activation energies of the different processes involved in surfactant-templating in zeolites was undertaken to increase our understanding of this approach.

In situ synchrotron XRD and pH measurements were recorded using the experimental setup shown in Figure 1a, which was specifically developed to *in situ* monitor mesostructuring procedure by synchrotron XRD. The reaction mixture, containing the basic surfactant solution ([NaOH] = 0.09 M; [CTAB] = 0.07 M) was placed in a sealed reactor while the temperature was carefully controlled (± 0.1 ºC) in the 45 – 90 ºC range. The USY zeolite (CBV 720, Si/Al = 15) was placed in the vessel on top of the reactor. Programmed opening of the lid between the reactor and the vessel allowed for the addition of the zeolite at once and thus the instant collection of data. Both pH and temperature probes were fitted in the reactor in order to continuously monitor both parameters. A peristaltic pump was used to circulate the mixture through a capillary where the XRD measurement was realized (see Figure S1 for further details).

The evolution of the pH was *in situ* monitored (Figure S2a) providing kinetic information on the OH^- consumption. These experiments were carried out after calibrating the pH glass electrode with titrated NaOH solutions at the different temperatures studied, see ESI for details (Figure S3).[9] The decrease in the OH^- concentration is due to both the cleaving of Si-O-Si bonds [9] and the ion exchange between H^+ and Na^+/CTA^+ ions in the zeolite. To distinguish between both processes, experiments in which the zeolite was firstly converted into its Na-form were carried out (Figure S2b) thus avoiding the ion exchange by H^+ ions during surfactant-templating. Similar results were obtained in both cases (Figure S2) and thus experiments obtained from the Na^+-form of the zeolite were employed in this case (Figure 1b). As deduced from the consumption of OH^- (Figure 1b) the cleavage of the Si-O-Si bonds is a very fast process, occurring within the first 5 min of the treatment. As previously described,[10] the opening of the Si-O-Si bonds and the formation of SiO^- sites is required for the mesostructuring to occur. Indeed, the process does not take place if base is not added to the reaction media (Figure S4) and the initial [OH^-] determines the amount of mesoporosity that can be formed within the zeolite.[10]

In order to obtain the apparent activation energy of this process, the cleavage of the Si-O-Si bonds, the calculation of the rate constant, k, at different temperatures was carried out from the slope of the linear part of the evolution of [OH^-] versus time. These values were used to depict the Arrhenius plot, from where the Arrhenius apparent activation energy was obtained, E_a^{OH-} = 35 kJ mol^{-1}

[a] Dr. N. Linares, Dr. E. O. Jardim, Dr. A. Sachse, Dr. E. Serrano, and Prof. Dr. J. Garcia-Martinez
Laboratorio de Nanotecnología Molecular, Departamento de Química Inorgánica
Universidad de Alicante
Ctra. San Vicente-Alicante s/n, E-03690 Alicante, Spain.
E-mail: j.garcia@ua.es; www.nanomol.es
[b] Prof. Dr. J. Garcia-Martinez
Rive Technology, Inc.
1 Deer Park Drive, Monmouth Junction, New Jersey 08852, United States

(Figure 2b, OH^- data).

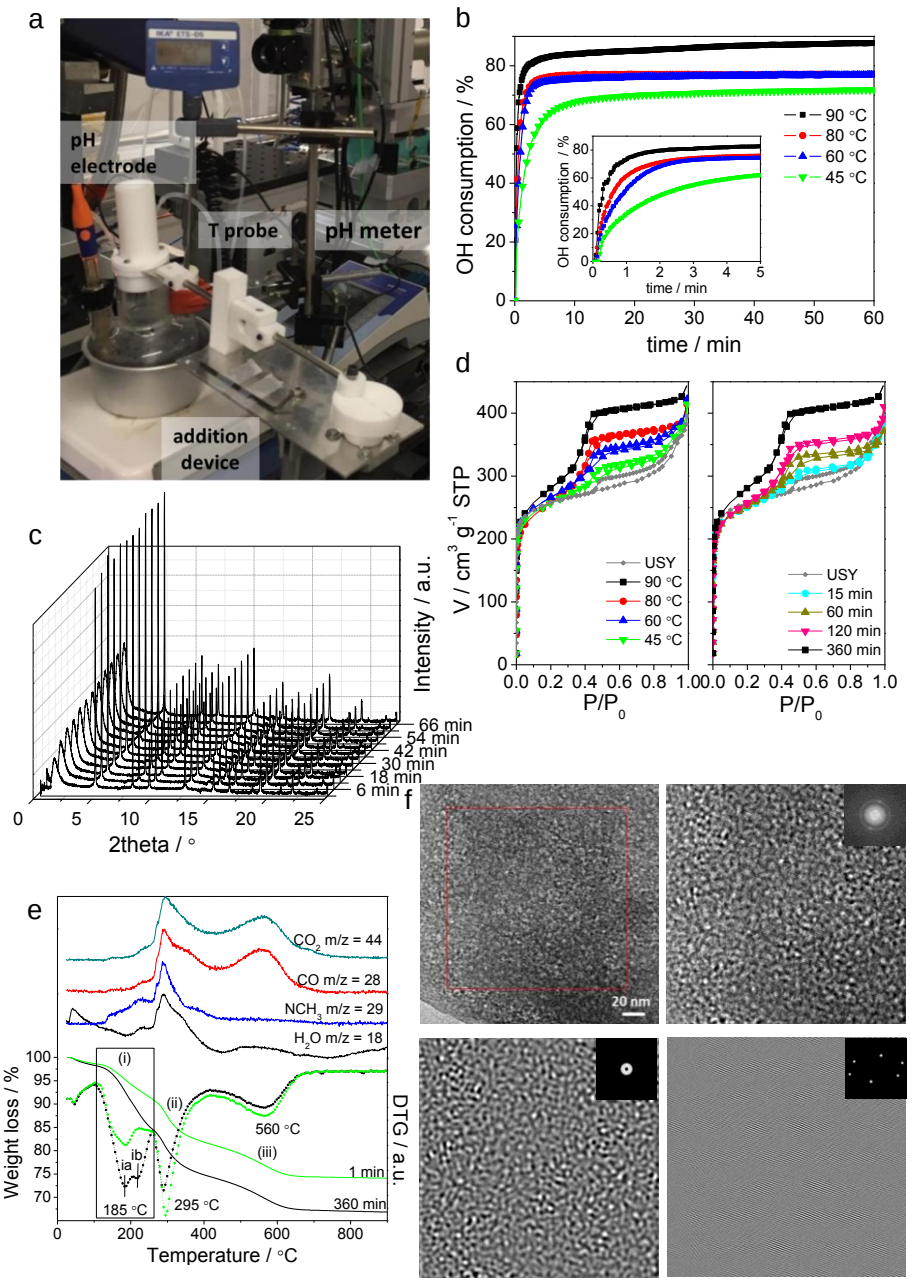

Figure 1. (a) Device used at the ALBA synchrotron, beamline BL04-MSPD, for the *in situ* synchrotron XRD. *Ex situ* experiments were also performed using this device. Evolution of the different parameters monitored during surfactant-templating of USY zeolite ([CTAB] = 0.07 M and [NaOH] = 0.09 M): (b) OH^- consumption profiles at different temperatures; (c) *in situ* time resolved synchrotron XRD patterns at 90 ºC; (d) N_2 adsorption/desorption isotherms at 77 K for the surfactant-templated USY zeolites at different temperatures and 360 min of treatment (left) and at different times at 90 ºC (right); (e) TG-DTG/MS measurements at the beginning (1 min) and the end (360 min) of the treatment at 90 ºC. The TGA (solid line) is presented below along with the DTG data (dashed line). Above are plotted various molecular species recorded from the MS measurements and their evolution with temperature; (f) (top left) TEM image of an ultramicrotomed surfactant-templated USY zeolite after 360 min of treatment at 90 ºC, (top right) reconstruction of the area marked by the red square from its corresponding FFT pattern (inset), (bottom left) mesopore structure of the selected area produced by masking the halo of the FFT pattern (inset) and (bottom right) crystalline structure of the area produced by masking the spots of the FFT pattern (inset).

To investigate the step related to the surfactant uptake by the zeolite, the amount of CTA^+ incorporated was monitored by TG. As an example, Figure 1e shows the TG-DTG/MS data of USY zeolite at the beginning (1 min, green line) and the end (360 min, black line) of the surfactant-templating treatment at 90 ºC. The calcination of CTA^+ in mesoporous materials involves three different steps:[11] (i) the elimination of the trimethylamine head group via Hofmann degradation (< 250 ºC); (ii) the oxidation of organic components (< 400 ºC), and (iii) a final oxidation process (> 400 ºC) during which carbonaceous species are removed. These three steps agree very well with the TG-DTG/MS data of surfactant-templated zeolites but also with those of a control experiment in which no base was added to the solution (Figure S5a) and of a physical mixture of zeolite and CTAB (Figure S5b). However, only when the surfactant and the base are present, and therefore the mesostructuring of the zeolite occurs, the peak corresponding to the first step (i) increases with the time of treatment, as shown in Figure 1e. When no base is used in the treatment and no mesostructuration of the zeolite occurs, the intensity of this peak remains mainly constant, see Figure S5a. Hence, the amount of CTA^+ removed in this first step (i) was associated as the CTA^+ responsible for the mesostructuring of the zeolite, more details are given in the ESI. Therefore, the percentage of CTA^+ removed in (i) (Figure S6) was used to determine the apparent activation energy of the process involving the uptake of CTA^+ associated to the SiO^- sites (Figure 2b, CTA^+ data), Ea^{CTA+} = 29 kJ mol^{-1}. Up to now, we have determined the apparent activation energies of two different steps included in the surfactant-templating of zeolites (see Figure 3). Following, apparent activation energies for the global surfactant-templating process were calculated through the evolving features observed using two independent techniques, namely, low angle XRD and N_2 physisorption. It should be noted that, , those are apparent energies and therefore only meaningful insights about their relative values can be drawn.

In situ synchrotron XRD experiments were performed using the experimental setup shown in Figure 1a. Diffractograms were recorded from 0.35 to 40 º*2θ* with time intervals of 2 min, allowing for the concurrent study of the kinetics of both the development of mesoporosity and the evolution of the crystallinity of the samples throughout the zeolite mesostructuring. The incorporation of surfactant-templated mesoporosity in USY can be inferred from the evolution of the peak in the low angle region of the diffractogram, at 1.6º *2θ*,[7] whose intensity increases throughout the experiment before reaching a plateau, indicating the completion of the mesostructuring process. In this study, mild reaction conditions were used to follow the early stages of this process with higher

accuracy. As an example, Figure 1c shows the *in situ* time resolved synchrotron XRD patterns of USY zeolite during surfactant-templating at 90 ºC, after a stable signal is reached. As presented in Figure 2a, the intensity of the peak at 1.6º *2θ* increases linearly with time, allowing for the calculation of the rate constant, k', of the mesostructuration process at different temperatures. These values were used to produce the Arrhenius plot shown in Figure 2b, from where the apparent activation energy of the development of mesoporosity was obtained, Ea_{Imeso} = 45 kJ mol^{-1}. Interestingly, this apparent activation energy is within the range of those obtained by measuring the linear growth rates of zeolites A (47.3 kJ mol^{-1}),[13a] X (62.6 kJ mol^{-1}),[13b] Y (49–65 kJ mol^{-1}),[13c] and silicalite-1 (42 kJ mol^{-1}),[13d] indicating that the energy necessary for the crystallization of the zeolites is similar to the one required for their mesostructuration via surfactant-templating (see Figure 3). These results confirm that the reorganization of FAU zeolite is energetically feasible under typical conditions of time and temperature involved in the synthesis and modification of zeolites. Exhaustive TEM analysis was also carried out to confirm the exclusive presence of intracrystalline mesoporosity and discard the formation of amorphous phases (see Figure 1f).

The formation of mesoporosity in zeolites can also be evaluated through *ex situ* N_2 physisorption of samples prepared using the same experimental setup at different times and subsequently calcined (see Figure 1d for their isotherms and Figure S7 for the evolution of their mesopore volume). The kinetics of the development of mesoporosity in USY zeolite as measured by gas adsorption follows the same trend than the previous analyses (Figure 2b), with an apparent Ea^{Vmeso} = 43 kJ mol^{-1}. The similarity between the apparent activation energies associated to the development of mesoporosity obtained by two independent techniques, XRD and gas adsorption, nicely supports the validity of these results.

In order to obtain further insights into the driving forces of the formation of intracrystalline mesoporosity in zeolites by surfactant-templating, *in situ* synchrotron XRD experiments were performed using different initial NaOH concentrations (0.06 and 0.09 M) and zeolites with varying Si/Al ratios (Si/Al = 15 and 40).

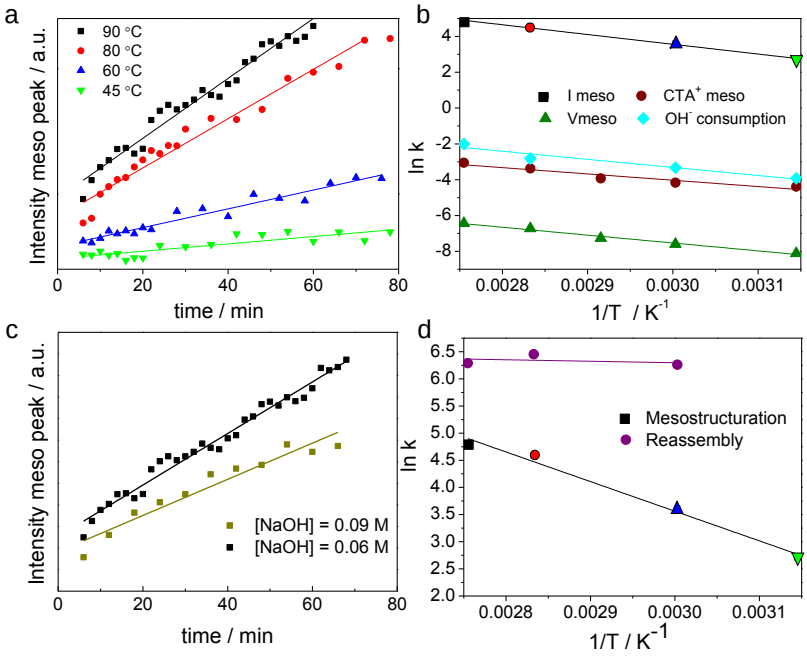

Figure 2. (a) Intensity profiles of the peak at 1.6º *2θ* (mesoporosity) during surfactant-templating at different temperatures (0.09 M NaOH). (b) Arrhenius plots obtained from the evolution of the different parameters associated to the development of mesoporosity in a surfactant-templated USY zeolite at 90ºC (0.09 M NaOH). (c-d) Intensity profiles of the peak at 1.6º *2θ* (mesoporosity) during surfactant-templating at 90 ºC and different NaOH concentrations, and (d) Arrhenius plots obtained from the I_{meso} profiles of the 1.6º *2θ* peak, comparison between surfactant-templating and dissolution + reassembly approaches (0.09 M NaOH).

As we have previously reported,[10] the OH^- concentration plays a major role in the incorporation of mesoporosity in the zeolite. Indeed, decreasing the initial NaOH concentration by two thirds (0.06 *vs* 0.09 M) decreases the rate of the development of mesoporosity almost in the same proportion at 90 ºC, see Figure 2c. On the contrary, zeolites with higher Si/Al ratios results in faster rates, see Figure S8. The stability of the zeolite towards basic cleavage increases with the Al content in the framework,[10] which results in rates almost 9 times slower for CBV 720 (Si/Al = 15) than CBV 780 (Si/Al = 40) at 60 ºC.

Finally, we have compared the kinetics of surfactant-templating with those of the dissolution and reassembly method, another very well known procedure which also uses CTAB as surfactant. The dissolution step was carried out in USY zeolite (Si/Al = 15) using a basic solution ([NaOH] = 0.09 M). The evolution of the concentration of OH^- was measured in order to study the cleavage of Si-O-Si bonds in the zeolite (Figure S9). In this case, the dissolution of the zeolite by OH^- ions has lower apparent activation energy than in the mesostructuring process, $E_a^{OH\text{-}dis}$ = 20 kJ mol^{-1} (Figure S9b). It is well-known that quaternary amines have a protective role for the zeolite, as evidenced also by the decrease in the intensity of the XRD peaks due to the crystallinity of the zeolite (blue lines in Figure S10).[7,14] In the second step (reassembly), CTAB was added to the mixture after 30 minutes. At this point the dissolved fragments precipitate immediately producing a very intense peak in the low angle region of the X-ray diffractogram (Figure S10, black lines). Moreover, the calculated rate of this second step barely changes with the temperature, resulting in a very low apparent activation energy ($E_a^{Imeso}{}_{reass.}$ < 1 kJ mol^{-1}) (Figure 2b). The distinctly different apparent activation energies of surfactant-templating and dissolution-reassembly suggest that the involved mechanisms are rootedly different (Figure 3). This conclusion is fostered by the different textural and chemical properties of materials obtained from both processes.

In conclusion:

(i) The formation of negatively charged Si–O^- species by OH^- ions is a very fast process that, however, present a significant apparent activation energy ($E_a^{OH\text{-}}$ = 35 kJ mol^{-1}), as it involves the cleavage of Si-O-Si bonds.

(ii) The incorporation of CTA^+ in the zeolite is carried out in two different stages. First, a very fast uptake of the surfactant by the zeolite surface takes place. After that, the amount of CTA^+ associated to the negatively charged Si-O^- sites in the zeolite increases

more slowly as the CTA^+ diffuses through the zeolite porosity. This electrostatic driven process is a less impeded step and presents lower apparent activation energy, E_a^{CTA+} = 29 kJ mol^{-1}.
(iii) The kinetics of the global process, which involves the formation of CTA^+ micelles within the zeolite crystals and the rearrangement of the crystal structure to accommodate them, is highly dependent on the temperature, consequently resulting in higher apparent activation energies, Ea^{Imeso} = 45 kJ mol^{-1} and Ea^{Vmeso} = 43 kJ mol^{-1}. These global apparent activation energies present similar values than those involved in the crystallization of zeolites,[13] hence confirming that the mesostructuring of FAU zeolite is energetically feasible under the conditions of time and temperature used in the synthesis of zeolites.

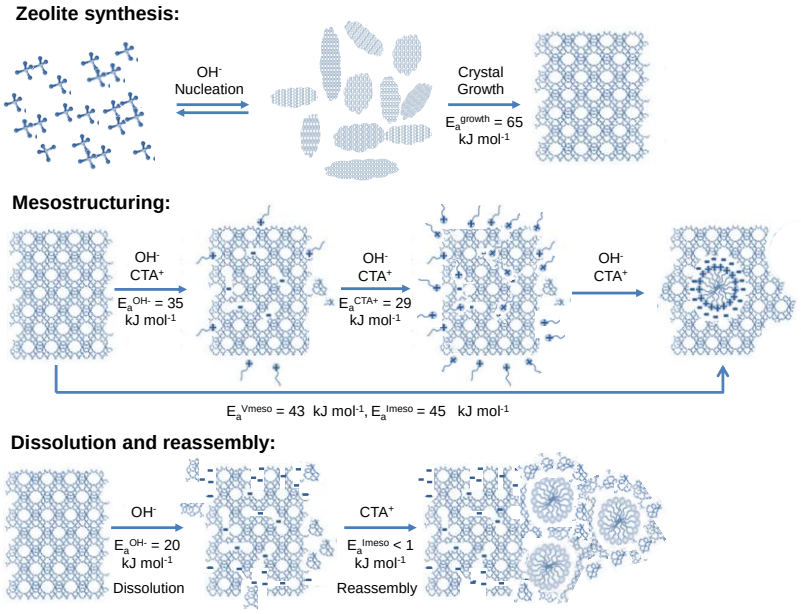

Figure 3. Schematic representation of the different procedures with USY zeolite namely, synthesis[13c] (above), mesostructuring (centre) and dissolution and reassembly (bottom), and the apparent activation energies of every process involved.

Acknowledgements

This work was supported by the Spanish MINECO and the EC through the ERA-NET CAPITA (AEI/FEDER, project WAVES, EP7-NMP-266543) and the ALBA Synchrotron (refs. 2016021622 and 2016021729). E.S. thanks the Spanish MINECO and AEI/FEDER, UE (CTQ2015-74494-JIN) and the UA (UATALENTO16-03). The authors thank Dr. C. Kamma-Lorger and F. Fauth (ALBA Synchrotron) for their assistance during the experiments, and J. Carpena and J.M. Martínez (UA) for assistance with the flow reactor design and construction.

Keywords: apparent activation energy, kinetics, mesoporous zeolites, surfactant-templating, synchrotron

[1] C.T. Kresge, M.E. Leonowicz, W.J. Roth, J.C. Vartuli, J. S. Beck, *Nature* **1992,** *359*, 710.
[2] a) C. Perego, R. Millini, *Chem. Soc. Rev.* **2013**, *42*, 3956. b) C. T. Kresge, W.J. Roth, *Chem. Soc. Rev.* **2013**, *42*, 3663.
[3] a) Y. Goto, Y. Fukushima, P. Ratu, Y. Imada, Y. Kubota, Y. Sugi, M. Ogura, M. Matsukata, *J. Porous Mater.* **2002,** *9*, 43; b) I. I. Ivanova, E. E. Knyazeva, *Chem. Soc. Rev.* **2013,** *42*, 3671; c) M. Choi, K. Na, J. Kim, Y. Sakamoto, O. Terasaki, R. Ryoo, *Nature* **2009,** *461,* 246.
[4] a) W. Park, D. Yu, K. Na, K.E. Jelfs, B. Slater, Y. Sakamoto, R. Ryoo, *Chem. Mater.* **2011,** *23*, 5131; b) J. Kim, M. Choi, R. Ryoo, *J. Catal.* **2010,** *269*, 219; c) M. Choi, H.S. Cho, R. Srivastava, C. Venkatesan, D.H. Choi, R. Ryoo, *Nat. Mater.* **2006,** *5*, 718.
[5] a) K. Li, M. Beaver, B. Speronello, J. Garcia-Martinez in *Mesoporous Zeolites* (Eds.: J.Garcia-Martinez, K. Li), Wiley-VCH, Weinheim, **2015**, pp. 321-348; b) A. Sachse, J. García-Martínez, *Chem. Mater.* **2017,** *29*, 3827.
[6] a) J. García-Martínez, M. Johnson, J. Valla, K. Li, J. Ying, *Catal. Sci. Technol.* **2012,** *2*, 987; b) J. García-Martínez, K. Li, G. Krishnaiah, *Chem. Commun.* **2012,** *48*, 11841; c) J. García-Martínez, C. Xiao, K.A. Cychosz, K. Li, W. Wan, X. Zou, M. Thommes, *ChemCatChem* **2014,** *6*, 3110; d) T. Prasomsri, W. Jiao, S.Z. Weng, J. García-Martínez, *Chem. Commun.* **2015,** *51*, 8900.
[7] N. Linares, A. Sachse, E. Serrano, A. Grau-Atienza, E. O. Jardim, J. Silvestre-Albero, M. A. Liutheviciene Cordeiro, F. Fauth, G. Beobide, O. Castillo, J. García-Martínez, *Chem. Mater.* **2016**, *28*, 8971.
[8] K. Li, J. Valla, J. García-Martínez, *ChemCatChem* **2014,** *6*, 46.
[9] J.C. Groen, GM. Hamminga, J.A. Moulijna, J. Pérez-Ramírez, *Phys. Chem. Chem. Phys.*, **2007**, *9*, 4822.
[10] A. Sachse, A. Grau-Atienza, E.O. Jardim, N. Linares, M. Thommes, J. García-Martínez, *Crystal Growth & Design* **2017,** *17*, 4289.
[11] F. Kleitz, W. Schmidt, F. Schüth, *Micropor. Mesopor. Mater.* **2001**, *44-45*, 95.
[12] a) V.R. Choudhary, S.G. Pataskar, *Thermochimia Acta*, **1986**, *97* 1; b) R.B. Borade, A. Clearfield, *Micropor. Mater.* **1996**, *5*, 289.
[13] S. P. Zhdanov, R. F. Gould, in: Molecular Sieve Zeolites – I, Advances in Chemistry Series (Eds.: S. P. Zhdanov, R. F. Gould), Vol. 101, ACS, Washington, DC, 1971, pp. 20–43; b) S. P. Zhdanov and N. N. Samulevich, in: Proceedings of the Fifth International Conference on Zeolites (Ed.: L. V. C. Rees), Naples, 1980, Heyden, London-Philadelphia-Rheine, 1980, pp. 75–84; c) H. Kacirek, J.H. Lechert, *Phys. Chem.* **1976**, *80*, 1291; d) B. J. Schoeman, J. Sterte, J.E. Otterstedt, *Zeolites* **1994**, *14*, 568.
[14] D. Verboekend, G. Vilé, J. Pérez-Ramírez, *Cryst. Growth Des.* **2012**, *12*, 3123.